# Plasma astrophysics

## Spectral analysis of time series (in-situ space data)

Data Analysis Report M2 IRT
2021-2022

Written by David Paipa *
Presented to Dr. Olga Alexandrova †

**December 6, 2021**
**PSL — Observatoire de Paris**

*. SUTS M2 IRT 2020-2021 . PSL - Obsevatoire de Paris. Meudon, France
†Observatoire de Paris. 5 place Jules Janssen 92190. Meudon, France

# Contents

# 1 Introduction

## 1.1 The solar wind and Earth's magnetosphere

The sun generates most of the activity in the interplanetary medium by irradiating the gas, dust and bodies orbiting its gravitational field with cosmic rays (electrons and protons, with some heavier atomic nuclei) and electromagnetic radiation along all the spectrum, ejecting into space 1 Million tons of Hydrogen per second in what we know as **solar wind**(SW)[1].

The SW coming towards the earth decelerates due to the interaction with earth's magnetosphere and diverts forming a hot dense boundary called the **bow shock**(BS), in front of the transition layer between the solar wind and earth's magnetopause, the **magnetosheath**(MSH). Beacuse of the interaction between the SW and the earth's magnetosphere, the magnetosheath is filled with complex plasma flow structures that can be described at large scales by MHD simulations. Variations due to small-scale structures in the plasma flows can result in discrepancies between the values of electric and magnetic field predicted by MHD and the ones measured in short time intervals[2].

Space probes sent into the MSH such as the CLuster Satellites are sensible to small scale structures given the comparison of scale with the MSH. As the spacecraft travels across these structures, having a way to estimate spectrum of localized events in time is useful to determine properties of these flows. Using scalograms and spectrograms the presence of pulses and oscillations can be identified, allowing to isolate these time lapses and studying the associate spectrum [3].

## 1.2 Discrete Fourier Transform (DFT)

U(t) is a series of N data points collected during a time $T = N\delta t$ where $\delta t$ is the minimum temporal resolution.

$$U(t_j) = U(t_0 + j\delta t); j \in [0, N) \tag{1}$$

The **Discrete Fourier Transform** performs a *scanning* in the $\omega$ frequency space looking for correlations between the signal and a set of orthonormal functions of the form $e^{i\omega t}$. Using the convolution to project the time series into this basis of functions, the DFT extract the necessary amplitude for each basis element when expressing the original signal as a lineal combination of these functions. For a discrete space, the DFT[1] that converts $U(t)$ into $\hat{U}(f)$corresponds to:

$$DFT[U(t)] = \hat{U}[f_n] = \frac{1}{N}\sum_{j=0}^{N-1} U[t_j]e^{-2i\pi\frac{nj}{N}} \tag{2}$$

Taking into account that the space of frequencies goes from $n = 0$ to $n = N - 1$ . This since the maximum frequency possible corresponds to an alternating series and the minimum value 0 corresponds to the "no oscillation" case or **mean value** of the series. Through the Fourier formality, time and frequency are conjugate variables, and since the FT is an invertible linear transformation the Inverse Discrete Fourier Transform (IDFT) is given by:

$$IDFT[\hat{U}(f)] = \hat{U}[t_j] = \sum_{n=0}^{N-1} \hat{U}[f_n]e^{2i\pi\frac{nj}{N}} \tag{3}$$

Time and frequency being **conjugate variables** leads to uncertainty when trying to determine both values accurately: longer samples of the signal in time may offer a more accurate estimate of the frequencies intensity (more frequency resolution $\delta t$), with the sacrifice of having a signal less localized in time, and viceversa. This can be better seen as:

$$\delta t \delta f \sim const. \tag{4}$$

Since data points in time and frequency are limited we have to work under the **assumption of periodicity** for finite signals

$$U[t_{j+N}] = U[t_j]; DFT[U(t)]_n = \hat{U}_n \tag{5}$$

This assumption can be reduced and re-interpreted as conjugation in time and frequency spaces, also understood as time and frequency reversal

$$DFT[U(T-t)]_n = \hat{U}_{N-n} \Rightarrow DFT[U(t)^*]_n = \hat{U}^*_{N-n} \tag{6}$$

[1] using the notation of [WELCH 1967]

Therefore in the case of real signal signal $U(t) \in \mathbf{R}$ where $U(t) = U^*(t)$ is true that

$$DFT[U(t)^*]_{N-n} = DFT[U(t)]_{N-n} = \hat{U}_n^* \tag{7}$$

## 1.3 Parserval's theorem

Let's assume a time series of N datapoints called $a(t)$ and its respective DFT's $A(f)$. Lets see the behavior of the integrated squared signal

$$\sum_{j=0}^{N-1} |U(t_j)|^2 = \sum_{j=0}^{N-1} U(t_j)U^*(t_j) = \sum_{j=0}^{N-1} \left( \sum_{n=0}^{N-1} \hat{U}(f_n) e^{-2i\pi \frac{nj}{N}} \right) \left( \sum_{m=0}^{N-1} \hat{U}^*(f_m) e^{2i\pi \frac{mj}{N}} \right) \tag{8}$$

Is important to take into account that for real signals $U^*(t)U(t) = U(t)^2$ and that projecting the signal on an orthonormal basis of functions implies $\sum_{j=0}^{N-1} e^{2\pi inj/N} e^{-2\pi imj/N} = N\delta_{n,m}$ .

$$\sum_{j=0}^{N-1} |U(t_j)|^2 = \sum_{j=0}^{N-1} [\hat{U}(f_0)\hat{U}^*(f_0) + \hat{U}(f_0)\hat{U}^*(f_1)e^{-2i\pi j/N} + \hat{U}(f_1)\hat{U}^*(f_0)e^{2i\pi j/N} + U(f_1)\hat{U}^*(f_1) + \dots] \tag{9}$$

But using the orthonormality principle we know that all terms with exponential components will disappear when adding over all $t_j$. Then, we are left with :

$$\sum_{j=0}^{N-1} |U(t_j)|^2 = [N\hat{U}(f_0)\hat{U}^*(f_0) + N\hat{U}(f_1)\hat{U}^*(f_1) + NU(f_2)\hat{U}^*(f_2)\dots] = N\sum_{j=0}^{N-1} |\hat{U}(f_j)|^2 \tag{10}$$

thus showing that,

$$\frac{1}{N}\sum_{j=0}^{N-1} |U(t_j)|^2 = \sum_{j=0}^{N-1} |\hat{U}(f_j)|^2 \tag{11}$$

## 1.4 Spectral Energy Density

For real signals the negative frequencies do not give additional information, and taking into account half of the spectrum is valid. For these, the sampled non-repeated frequencies are given by

$$f_n = n/T; n = 0, 1, 2...N/2 \tag{12}$$

from this we can know that the minimum frequency possible is 0 but also that the maximum frequency is $\frac{N}{2T} = \frac{1}{2\delta t}$. The energy distribution in the frequency signal (Power Spectral Density PSD) in this frequencies is given by

$$S[f_n] = 2T|\hat{U}(f_n)|^2; N = 0, 1, 2...N/2 \tag{13}$$

Applying Parseval's theorem in Eq.11 with the new definition of $S[f_n]$ we get that

$$2\delta t \sum_{j=0}^{N-1} |U(t_j)|^2 = \sum_{j=0}^{N-1} S(f_j) \tag{14}$$

Taking into account that $T = 2\delta t$. If the signal $U(t)$ is in function of time (measured in seconds $[s]$), and with amplitude measured in arbitrary units $[\chi]$, the signal $\hat{U}(t)$ is given as a function of $[s]^{-1} = [Hz]$. The energy distribution magnitude is given in $[\chi]^2[Hz]$

## 1.5 Windowed DFT: an approach in frequency and time

The analyzed signal is **split** [2] into $M$ pieces of length $m$ such that $N = mM$. For each piece a DFT is performed, giving $M$ different spectra containing up to $m$ frequencies. The window's shape can be a cutoff

[2] This is the special case when $m$ divides $N$ without residues. This can be extended to a general case when the residues are appended to one (or many) of the groups in order to perform the analysis (under the correct normalization) or, if needed, can be removed in the windowed DFT.

in the signal (the case of a Box Car window) of different shapes depending on the characteristics needed (Barlett, Hamming, Blackman among them)[4].

This Approach can provide not just a 1D spectra in frequency space but resolution in frequency and in time as well. Form the information previously mentioned, and specially from the stated in Eq. 4 one can infer that more data points $m$ per interval imply **increasing resolution in frequency** space. But using more points implies as well a lower number of intervals $M$ which **decreases resolution in time**. A representation of the spectral energy density in the frequency-time space is called a **spectrogram**.

# 2 Development

## 2.1 Analysis of synthetic signals

### 2.1.1 Single signal $y_0$

To begin simple lets analyze a synthetic sinusoidal signal of the form

$$y_o(t) = A_o \sin(2\pi f_o t) \tag{15}$$

where the selected amplitude and frequency are $A_o = 2$ and $f_o = 0.02$. The signal has $N = 10^3$ points and for simplicity $\delta t = 1$, resulting in a range of frequencies from 0 to 0.5 .

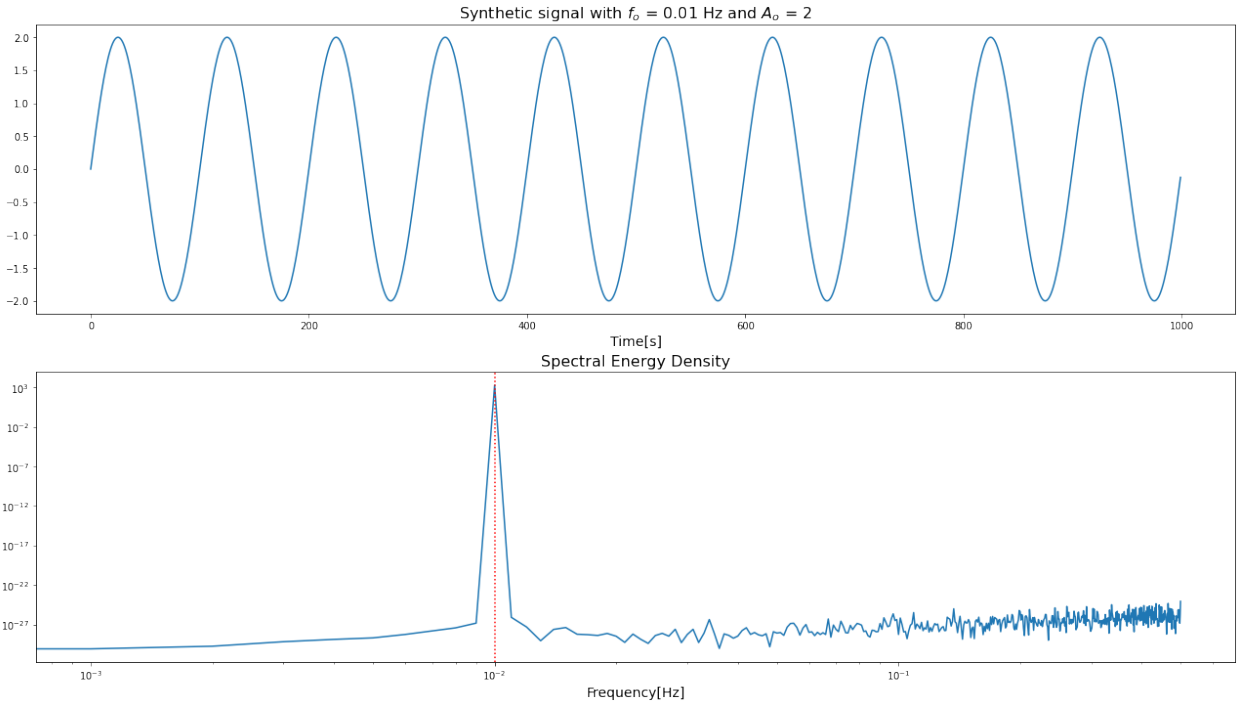


Figure 1: Synthetic sinusoidal signal $y_0$, with amplitude $A_0$ and frequency $f_0$, and its respective PSD $\sim |\hat{y_0}|^2$. The used frequency $f_0$ is pointed in red, and is notorious how the DFT highlights this specific frequency, being this various order of magnitude more powerful than the other frequencies.

Is safe to assume that the PSD integral is reduced to a $\delta(f)$ function centered in $f_o$ since the PSD is many order of magnitude higher here than in other part of the spectrum , therefore,

$$\sum_f PSD \sim max(PSD) * (1/\delta t)$$

To check Parseval's theorem using Eq.14 I used the analytical solution[3] of the integral of $y_0$ to calculate

$$\sum_t |y_0|^2 = \sum_{j=0}^{N-1} |y_0(t_j)|^2 \approx \int_0^{t_n} (A_o \sin(2\pi f_o t))^2 dt \approx 1000 \tag{16}$$

[3]This approximation is valid for large N

then, calculated a ratio $Q$ to quantify how much both sides of Eq. 14 are alike

$$Q = 2\delta t \frac{\sum_t y_0}{max(PSD(y_0))} \tag{17}$$

So that when $Q = 1$ the Parseval relation holds. using this and knowing that the maximum PSD value (in $f_0$) is 2000, Q is indeed 1 and the theorem validates the procedure, showing that energy is conserved with the transformation.

### 2.1.2 Combined signals $y_1$ and $y_2$

Now, a second set of parameters in Amplitude $A_1 = 0.8$ and Frequency $f_1 = 0.08$ are used to generate two more synthetic signals $y_1(t)$ and $y_2(t)$ with the form:

$$y_1(t) = A_o sin(2\pi f_o t) + A_1 sin(2\pi f_1 t) \tag{18}$$

$$y_2(t) = \begin{cases} A_o sin(2\pi f_o t) \text{ if } t < T/2 \\ A_1 sin(2\pi f_1 t) \text{ if } t \geq T/2 \end{cases} \tag{19}$$

The PSD for each signal is displayed in Figure 2 where in each case the selected frequencies are highlighted by the DFT displaying peaks. In the case of $y_1(t)$ the peaks approximate a $\delta$ function again and overcome the rest of the spectrum by many order of magnitude, while in the case of $y_2(t)$ the peaks are barely one order of magnitude higher than the perturbations in the rest of the spectrum.

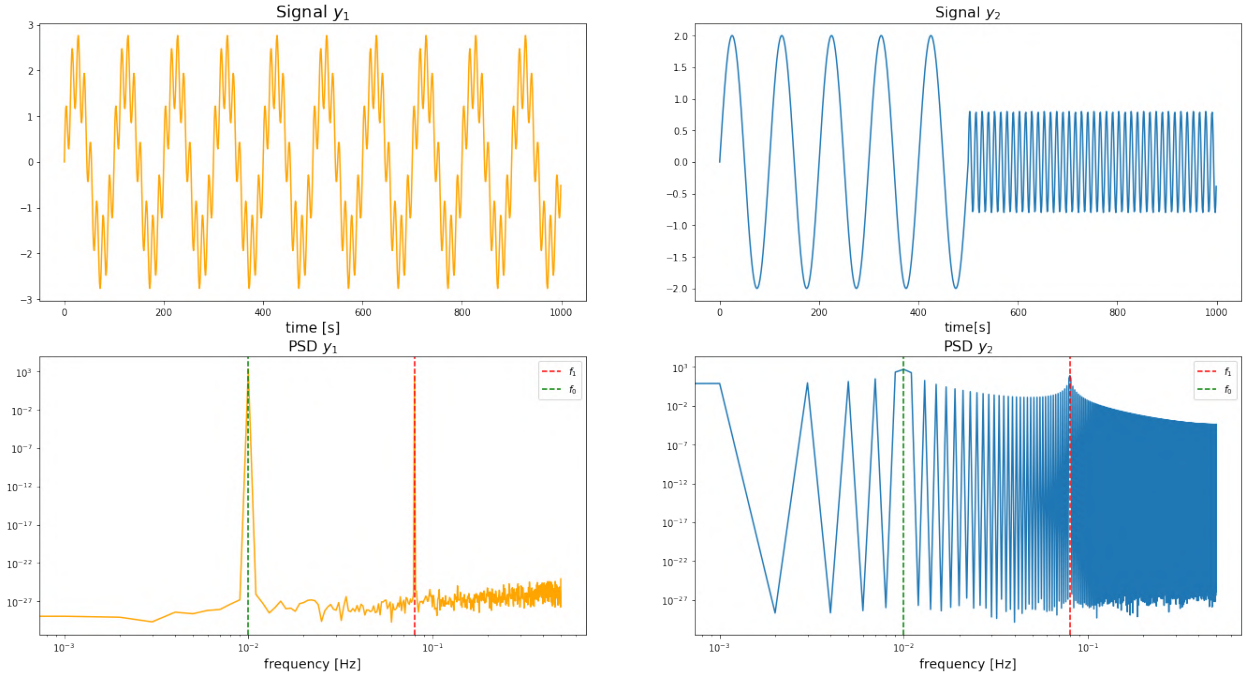


Figure 2: Synthetic sinusoidal signals and their respective PSD . The frequencies $f_0$ and $f_1$ are highlighted. The peaks align correctly with the used frequencies hence showing again the DFT's ability to find frequencies, but the shape of the signal seems to be relevant for the magnitude and shape of the rest of the spectrum.

This perturbations in the PSD can be explained by the discontinuity present in $y_2(t)$ at $t = T/2$. In the discontinuity point the inner product of functions with frequencies different to $f_1$ and $f_2$ is not always zero, moreover, a sharp discontinuity might imply the sum of infinite relevant frequencies to approximate the discontinuity point.

### 2.1.3 Morlet Wavelet Analysis

With the the Wavelet Analysis we now use a family of functions that are not orthonormal such as the family generated by the Morlet Mother Wavelet:

$$\psi_0(t) = \pi^{-1/4} e^{-iw_o t} e^{-t^2/2} \tag{20}$$

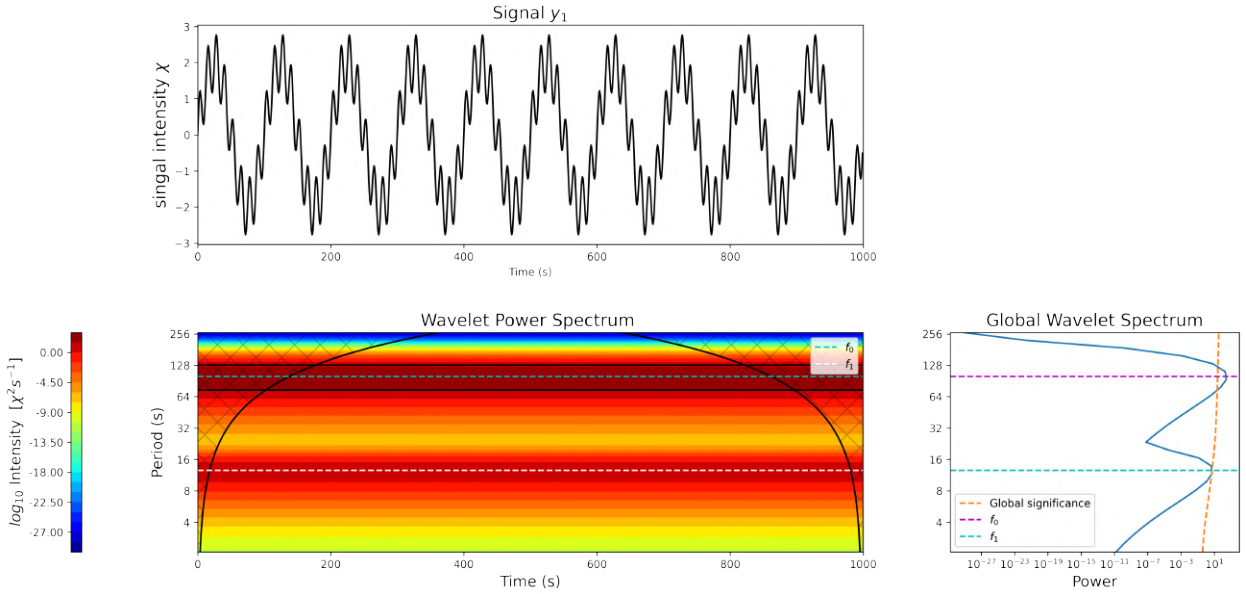


Figure 3: Synthetic signal $y_1$ and its scaleogram made with Morlet wavelet Transform . The frequencies $f_0$ and $f_1$ are highlighted during the totality of the signal's duration. The peaks in the Global Power Spectrum align with the used frequencies ( periods $\tau_o = 100$s and $\tau_1 = 12.5$s), corresponding to the relation $1/f \approx \tau$

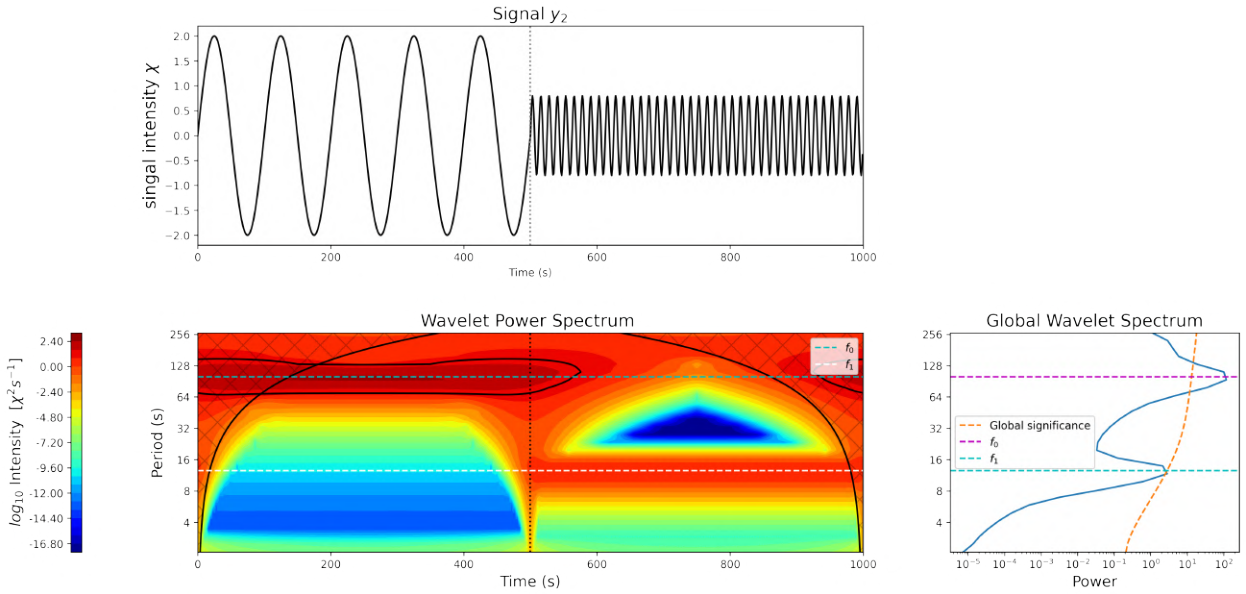


Figure 4: Synthetic signal $y_1$ and its scaleogram made with Morlet wavelet Transform . The frequency $f_0$ is highlighted for the first half of the signal's total duration and $f_1$ during the other half, having a perturbation in all frequencies (discontinuity) around $t = T/2$ . The peaks in the Global Power Spectrum align with the used frequencies, but the shape of the spectrum is different from the shape of the spectrum of $y_1$

### 2.1.4 Comparing

When analyzing both signals under the Morlet wavelet Transform in figures 3 and 4 its easy to note the great advantage of the Wavelet Transform: information in time and frequency of localized events. This can be deduced from the formulation of the transform where $U(t) \Rightarrow W(\tau, t)$ where a signal in parametrized in time should now be expressed as a function of time and scale (period). In this aspect, Fourier is left behind given that is can only transform the signal from time domain to exclusively frequency domain $U(t) \Rightarrow \hat{U}(f)$.

On the other hand, since DFT do not subdivide the signal, it can have up to $N/2$ frequencies, in this case ranging from 0Hz to 0.5Hz, while the Morlet Wavelet Transform has less resolution in frequency(scale) space with frequencies ranging from $0.0037 \approx 0$Hz to $0.484 \approx 0.5$Hz, with the approximation being valid for a conversion factor of 1.03 (consequence of the relation $1/f \approx \tau$ that holds for the parameters chosen).

For the cases show previously, the information discussed is summarized on The table 1

| **Transform** | **DFT** | **Wavelet** |
|---|---|---|
| # frequencies. | 500 | 29 |
| # time bins | 1 | 1000 |
| max freq | 0.5 Hz | 0.484 Hz |
| min freq | 0 Hz | 0.003 Hz |
| inputs | f | t,$\tau$ |

Table 1: General quantitative overview of the DFT comared to the Wavelet Transform on the framework of signals $y_1$ and $y_2$

## 2.2 In Situ data analysis

The case of study is an observation made by the **Cluster Satellites** while repeatedly[4] crossing Earth's bow shock, measuring magnetic field B [nT] components (XYZ) for a time lapse of $T \approx 4.5$ hr and with a sampling frequency of $1/\delta t \approx 25Hz$, meaning a high number of data points $N \approx 4 \times 10^5$.

### 2.2.1 Definition of regions

The goal is to analyze three different scenarios under the lens of the Wavelet and Fourier Transforms: numerous flows of plasma in the **magnetosheath** (MSH), a less turbulent and dense region exposed to **solar wind** (SW) and the boundary between both, the **bow shock** (BS). Thanks to the large scale of the BS, the local curvature is low at the crossing point in the orbit of the Cluster satellite, and the velocity vector is perpendicular to the boundary surface when crossing the BS. Three windows are selected in time in order to perform the analysis:

- **Region I** contains data from the probe into the interior of the MS
- **Region II** contains a discontinuity corresponding to crossing the BS
- **Region III** corresponds to data from the probe exposed to SW

### 2.2.2 Exploring the Data

First, lets take a look at the raw data and any notorious phenomena it may present. The magnetic field Vector $\vec{\mathbf{B}}$ is reconstructed: the magnitude $|\vec{\mathbf{B}}|$, polar angle $\theta$ and azimuth angle $\phi$ are displayed as well in figure 5 knowing[5] that

$$
\begin{aligned}
|\vec{B}| &= \sqrt{B_x^2 + B_y^2 + B_z^2} \\
\phi &= \arctan(B_y/B_x) \\
\theta &= \arccos(B_z/|\vec{B}|)
\end{aligned}
\tag{21}
$$

As a note I would like to clarify that despite the workshop requested analysis over the signal $B_x$ I found that using the radius $|\vec{B}|$ and orientation $\phi$,$\theta$ of the magnetic vector is convenient to separate the observed phenomena in magnitude and direction.

[4] Since the solar wind and earth's magnetic field are not static, the boundary of shock is not steady and moves faster than the satellites, crossing them many times when they are around its average position.

[5] Considering that for $\phi$ the arctan function diverges depending on the sign of $B_x$

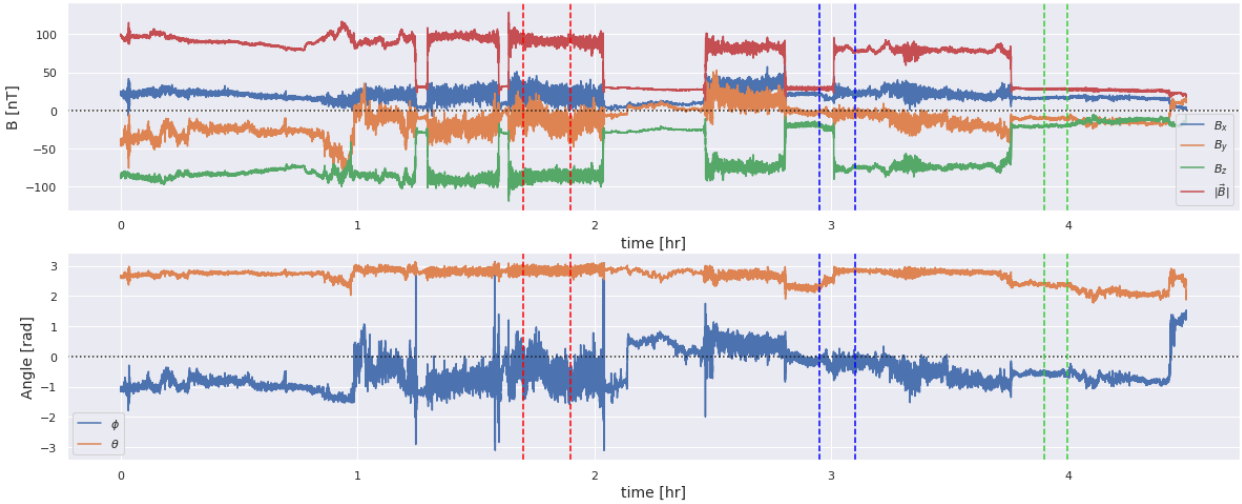


Figure 5: Raw data for the three components of the magnetic field $B_x$, $B_y$ and $B_z$. The magnetic field vector magnitude and direction are expressed in spherical coordinates by $|\vec{\mathbf{B}}|$, $\phi$ and $\theta$. Since the azimuth angle is periodic, discontinuities are present when $\phi$ increases from angles a slightly smaller to $2\pi rad$ to small values above 0 rad. The Regions are delimited by the vertical dashed lines: Region I delimited by red lines, the Region II by the blue lines and the Region III by the green ones.

The magnitude of the measured magnetic field $|\vec{B}|$ is a way of combining all three measurements into a single value of physical relevance. When analyzing the Fourier PSD of $|\vec{B}|$ against frequency $f$ along all the signal one realizes that if follows linear trends on two different parts of the spectra with fitted slopes of $-1.58$ and $-2.36$ as reported in figure 6

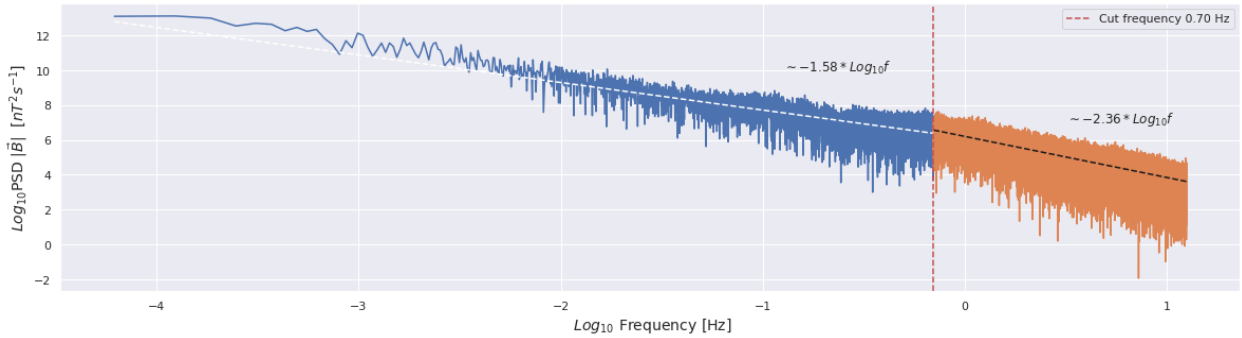


Figure 6: Power spectral density using Fourier Analysis of the magnitude of the magnetic field $|\vec{B}|$ along all the 4.5hr period. The spectrum is cut in two pieces of different slopes using as cutting frequency the peak frequency $f_3 = 0.7$ Hz found in figure 8.

### 2.2.3 Region I: Magnetosheath

Region I is taken between 1.7hr and 1.9hr from the $t_o$, where the first thing jumping to sight is the high variance in the measurement of the magnetic field. It's worth highlighting that there are no visible boundaries in the data (such the case of Region II). When performing the wavelet transform to the signal, a scalogram is built, which represent the intensity of correlation of stretched mother wavelets with a localized interval of the signal.

In the scalogram of Region I many features are visible around the highlighted key frequencies (periods) which are found in further steps. This is due to the fact that the spacecraft is moving through cyclotron ans sheet structures formed inside the magnetosheath, which have oscillation frequencies associated [5]. For analyzing punctual events I splitted the Region I $|\vec{B}|$ signal in many sections and selected a piece of signal

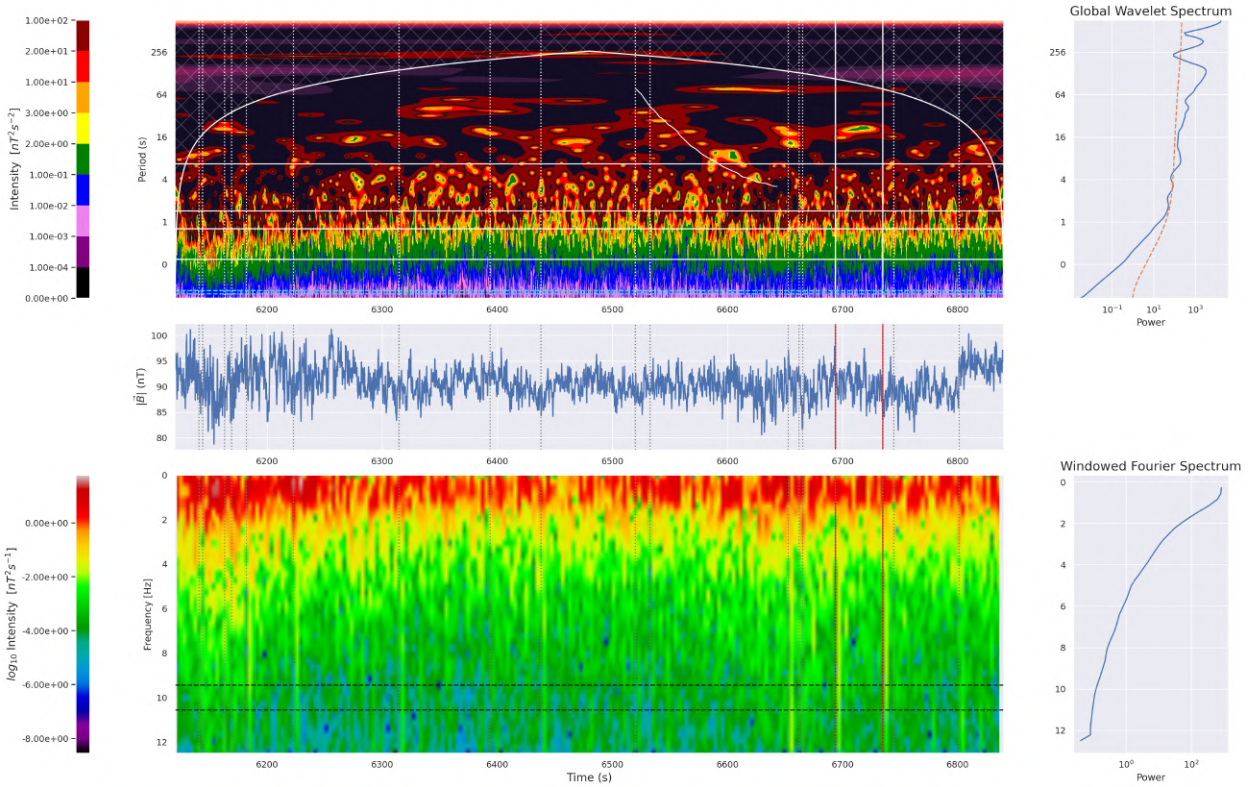


Figure 7: magnetic field magnitude $|\vec{B}|$ in Region I represented with the wavelet and windowed Fourier spectrum analysis. The top panel has the Morlet Wavelet Scalogram of the signal and the global (time-integrated) spectrum on its right. A possible structure in the scalogram is identified by accident (better seen with PAUL basis) between $t = 6520$ s and $t = 6650$ s. In the middle panel the signal corresponding to the magnitude of local magnetic field $|\vec{B}|$. On the bottom, the Windowed Fourier spectrogram with a time resolution of $\delta t = 2.88$s. The integrated windowed spectrum is plotted to the right. The splits in time are made using the method described in section A.1 with parameters $\tau_c = 10$ Hz and $\eta = 1.12$ Hz and the associate frequency band is displayed in the Fourier spectrogram (black) and the Morlet scalogram (cyan). The three frequencies pointed in white in the Wavelet scalogram are defined in figure 8 and are organized from top to bottom being $f_4$ the last one. The section Highlighted in red is used for further analysis and goes from $t = 6610$ s to $t = 6695$ s.

corresponding to the highlighted section in Figure 7 for studying the spectral properties in more detail with the Fourier Transform. When the Fourier analysis is made, there are features that are worth mentioning:

- Peaks are found in all three spectra at $f_1 = 0.15$ Hz
- A Drop in all three spectra at $f_2 = 0.7$ Hz
- Anomaly (possible drop) at $f_3 = 1.25$ Hz
- A peak in $\phi$ at $f_4 = 3.4$ Hz

I chose this section given that it has a enough length to provide good spectral resolution and has multiple features at different frequencies (periods) of the scalogram. Note how at $f_3$ the spectra displayed in figure 8 changes in slope. For analyzing the slope of the spectra is split the spectra in 2 qround $f_3$ and fit different linear regressions on each one in the log-log space as shown in figure 6.

The Wavelet power spectrum $|W^2(f)|$ with the used scale and $omega_o$ and the Fourier spectrum $S(f)$ are similar. This is displayed in the Figure 9. As expected, the wavelet spectrum has less spectral density since the information contained in the temporal dimension was lost by integrating over time. The uncertainty again plays an important role, limiting the resolution in frequency when acquiring some information along time.


Figure 8: The section highlighted in figure 7 is isolated. The previous and next pieces of signal are named section 1 and 3 respectively, while the selected section is labeled section 2. (Top Panel) behavior of the direction of the magnetic field in each section, putting in evidence what seems to be cyclic curved movements around a central position. The zero coordinate associated with $\phi$ is phased for section 1, 2 and 3 by 2, 4 and 6 units respectively in order to avoid overlapping. (Both middle panels) The 3 sections of the used signal are displayed and the section 2 is isolated and shown as well. (Bottom panel) Fourier Spectrum of the magnetic field magnitude $|\vec{B}|$ and direction $\theta$,$\phi$ for the selected section where coincident peaks and anomalies are pointed, corresponding to frequencies of $f_1 = 0.15$ Hz , $f_2 = 0.7$ Hz ,$f_3 = 1.25$ Hz and $f_4 = 3.4$ Hz. These four frequencies are displayed in white in figure 7

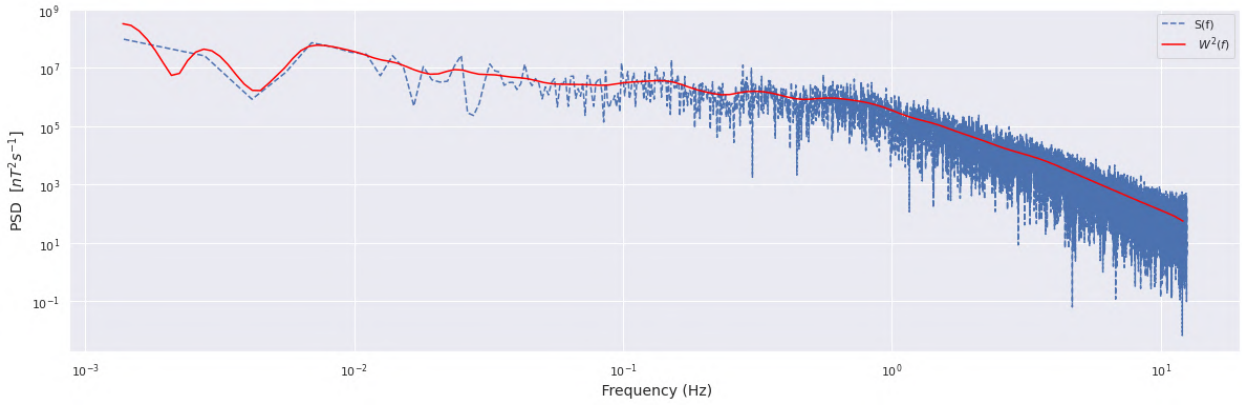


Figure 9: Relation of the squared wavelet transform and the Power spectral density of Region I.

### 2.2.4 Region II: Bow Shock

When crossing the bow shock a big discontinuity is evident in scalogram in fiugre 10 as it splits the timeline into a previous state exposed to solar wind and a posterior state inside the magnetosheath. In this case I analyzed with Fourier the section around the discontinuity due to the boundary crossing. Since it's a discontinuity I don't expect to have a particular frequency highlighted by the Fourier power spectrum but It's worth analyzing this section anyway. Also note how section 3 (corresponding to the magnetosheath) has

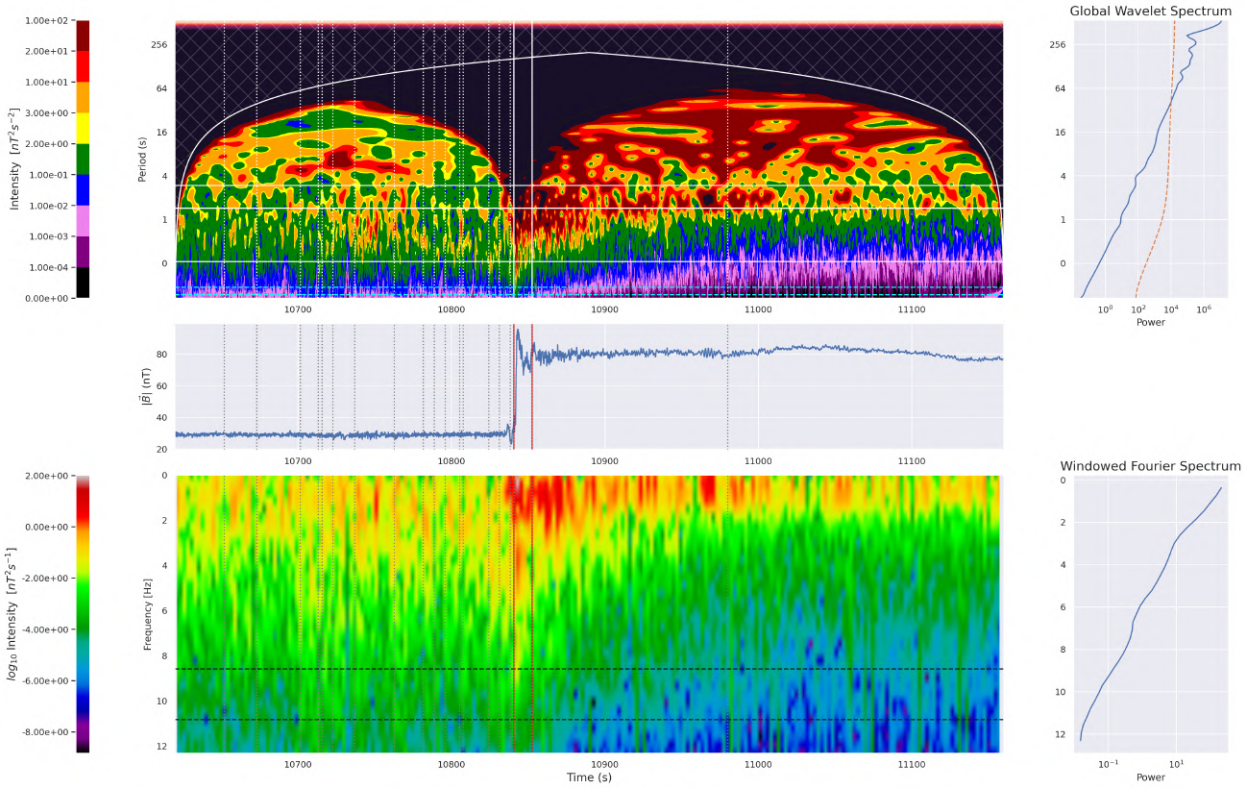


Figure 10: magnetic field magnitude $|\vec{B}|$ in Region II represented with the wavelet and windowed Fourier spectrum analysis with the same sections and definitions of figure 7. The Windowed Fourier spectrogram has a time resolution of $\delta t = 2.88$s. The splits in time are made using the method described in section A.1 with parameters $\tau_c = 9.7$ Hz and $\eta = 2.24$ Hz and the associate frequency band is displayed in the Fourier spectrogram (black) and the Morlet scalogram (cyan). The three frequencies pointed in white in the Wavelet scalogram are defined in figure 11. The section Highlighted in red is used for further analysis and goes from $t = 10830$ s to $t = 10855$ s.

this defined quasi-circular trajectories in the direction map $\phi$ vs $\theta$, while the sections corresponding to solar wind and boundary do not have this behavior.

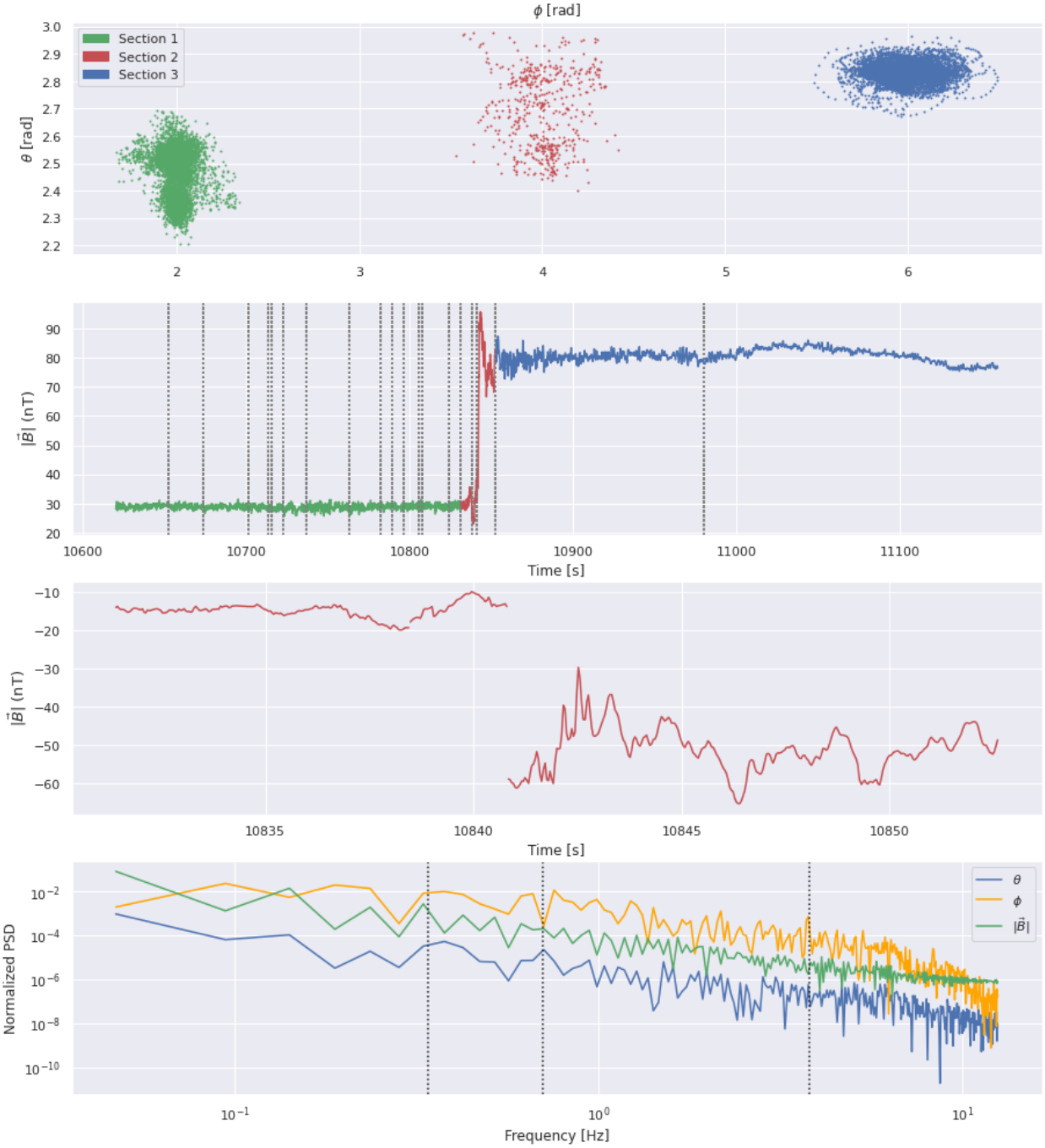


Figure 11: The section highlighted in figure 10 is isolated and analyzed similar to the results in Figure 8. (Top Panel) behavior of the direction of the magnetic field in each section. The zero coordinate associated with $\phi$ is phased for section 1, 2 and 3 by 2, 4 and 6 units respectively in order to avoid overlapping. (Bottom panel) Fourier Spectrum of the magnetic field magnitude $|\vec{B}|$ and direction $\theta$,$\phi$ for the selected section where coincident peaks and anomalies are pointed, corresponding to frequencies of $f_1 = 0.34$ Hz (peak in all 3 spectra), Hz ,$f_2 = 0.7$ Hz (drop $\phi$ and peak $\theta$) and $f_3 = 3.8$ Hz (peak in $\phi$ spectra). These four frequencies are displayed in white in figure 10

### 2.2.5 Region III: Solar Wind

The solar wind can show frequencies associated with fast corrotating streams shaped by the magnetic lines of the sun's huge magnetic field. The scalogram in figure 12 show less small localized structures than the case of the magnetosheath, but more diffuse wavelet resonances at higher periods. I chose a section with high intensity fluctuations at different periods in the scalogram to be analyzed with FT. Some resonant frequencies are proposed based on anomalies visible in the spectrum of the chosen section.

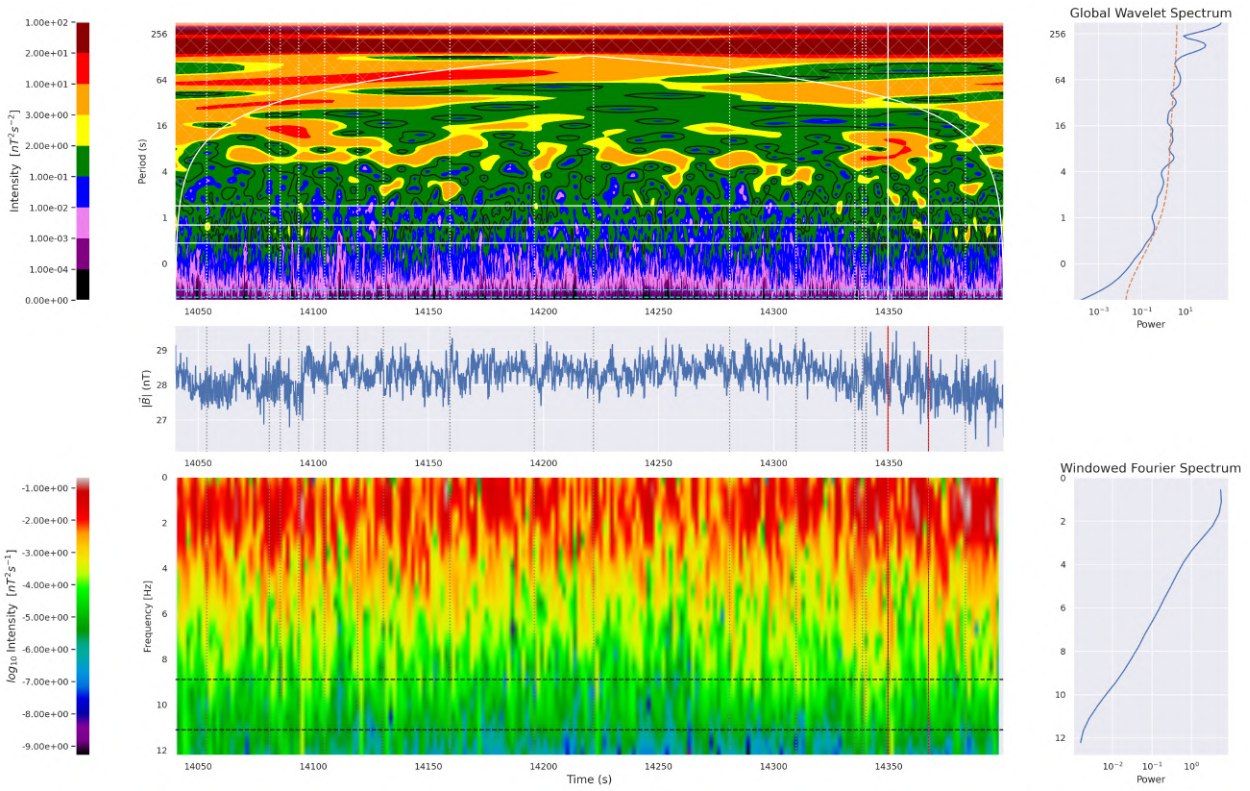


Figure 12: magnetic field magnitude $|\vec{B}|$ in Region III represented with the same sections and definitions of figure 7. The Windowed Fourier spectrogram has a time resolution of $\delta t = 2.88$s. The splits in time are made using the method described in section A.1 with parameters $\tau_c = 10$ Hz and $\eta = 2.22$ Hz and the associate frequency band is displayed in the Fourier spectrogram (black) and the Morlet scalogram (cyan). The three frequencies pointed in white in the Wavelet scalogram are defined in figure 13. The section Highlighted in red is used for further analysis and goes from $t = 14040$ s to $t = 14400$ s.

# 3 Conclusions

When aiming to identify the properties of short-timed pulses or oscillations,the use of wavelet transform in the analysis of in-situ measurements of the magnetic field showed to be really useful to isolate the events that are visible in a scalogram. The frequencies highlighted for the studied section inside the MSH are poorly similar to the ones reported in [5] but are notorious features of the spectra nonetheless.

The Windowed Fourier spectrum can not provide as good resolution and information quality as the wavelet transform scalogram, but can be handy for analyzing already isolated events. The Fourier windowed function can be used to define the boundaries of the events under the assumption that discontinuities in the signal require contributions along all the spectrum to be approximated. This can be tricky since not all isolated events have to be consequent with a discontinuity on the signal. In the BS boundary changes in direction are evident when studying the system in spherical coordinates. Considering the magnetic field in the basis of the normal and perpendicular directions to the BS surface can provide more physical information on the direction of the field [5]. Studying the magnitude of the magnetic field instead of a single direction was intended to consider all data available, but it is also true that precesion of the direction vector of the local

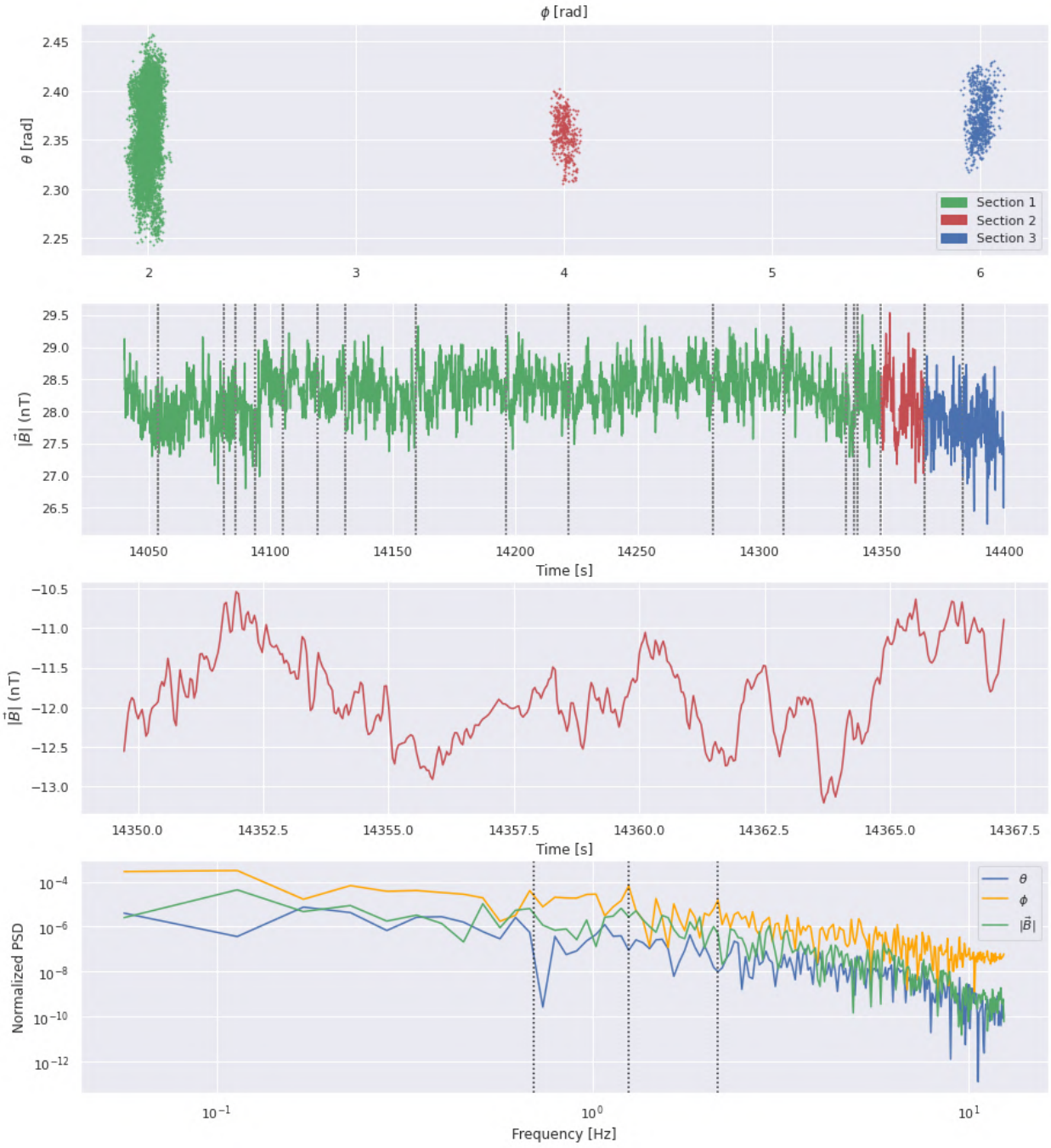


Figure 13: The section highlighted in figure 12 is isolated and analyzed similar to the results in Figure 8. (Top Panel) behavior of the direction of the magnetic field in each section. The zero coordinate associated with $\phi$ is phased for section 1, 2 and 3 by 2, 4 and 6 units respectively in order to avoid overlapping. (Bottom panel) Fourier Spectrum of the magnetic field magnitude $|\vec{B}|$ and direction $\theta$,$\phi$ for the selected section where coincident peaks and anomalies are pointed, corresponding to frequencies of $f_1 = 0.7$ Hz (drop $\theta$ and peaks in magnitude and$\phi$), Hz ,$f_2 = 1.25$ Hz (peak in $\phi$) and $f_3 = 2.15$ Hz (drop $\theta$ and peaks in magnitude and$\phi$). These four frequencies are displayed in white in figure 12

field around a central position would not be reflected. It is important to consider direction and magnitude in exercises as the identification of key frequencies when observing the spectra of the selected sections.

# References


[1] N. Meyer-Vernet, "Basics of the solar wind," *Meteoritics and Planetary Science vol. 43 iss. 11*, vol. 43, nov 2008.

[2] L. Rakhmanova, M. Riazantseva, and G. Zastenker, "Plasma and magnetic field turbulence in the earth's magnetosheath at ion scales," *Frontiers in Astronomy and Space Sciences*, vol. 7, p. 115, 2021.

[3] G. Paschmann and P. W. Daly, "Analysis Methods for Multi-Spacecraft Data. ISSI Scientific Reports Series SR-001, ESA/ISSI, Vol. 1. ISBN 1608-280X, 1998," *ISSI Scientific Reports Series*, vol. 1, Jan. 1998.

[4] K. M. M. Prabhu, *Window Functions and Their Applications in Signal Processing.* CRC Press/Taylor Francis, 2013.

[5] O. Alexandrova, A. Mangeney, M. Maksimovic, C. Lacombe, N. Cornilleau-Wehrlin, E. Lucek, P. Décréau, J.-M. Bosqued, P. Travnicek, and A. Fazakerley, "Cluster observations of finite amplitude Alfvén waves and small-scale magnetic filaments downstream of a quasi-perpendicular shock.," *Journal of Geophysical Research Space Physics*, vol. 109, no. A5, p. A05207, 2004.

# Appendices

## A Methods

### A.1 Identifying discontinuities

When decomposing signal discontinuities in time using Fourier, the discontinuity point usually requires contributions from many parts of the spectrum to approximate the sharp point. In the Windowed Fourier spectrogram in Figure 7 this can be seen for higher frequencies as vertical lines of higher intensity in the points where the discontinuities are.

I used this fact to find splitting points that may indicate an unseen boundary in the conditions of the signal, which are not as notorious as the case of Region II. The algorithm is:

- Create a windowed Fourier Spectrogram of the requested region.
- Find in the Wavelet spectrogram a target frequency $\tau_c$ (period) in which variations along time are evident and recurrent.
- Define an **utility bandwidth** $\delta\tau$ around $\tau_c$ ($\tau_c \pm \delta\tau$) in which the localized phenomena are contained
- integrate (sum) the contributions of all frequencies contained in the utility bandwidth applied on the Fourier spectrogram, resulting in a time series of the intensity of this band.
- Using discrete differentiation over the resulting time series, identify all sudden changes in slope that exceed in magnitude a defined threshold $\eta$
- the position of the points where the changes in slope exceed the threshold. these are the position of the splitting points.

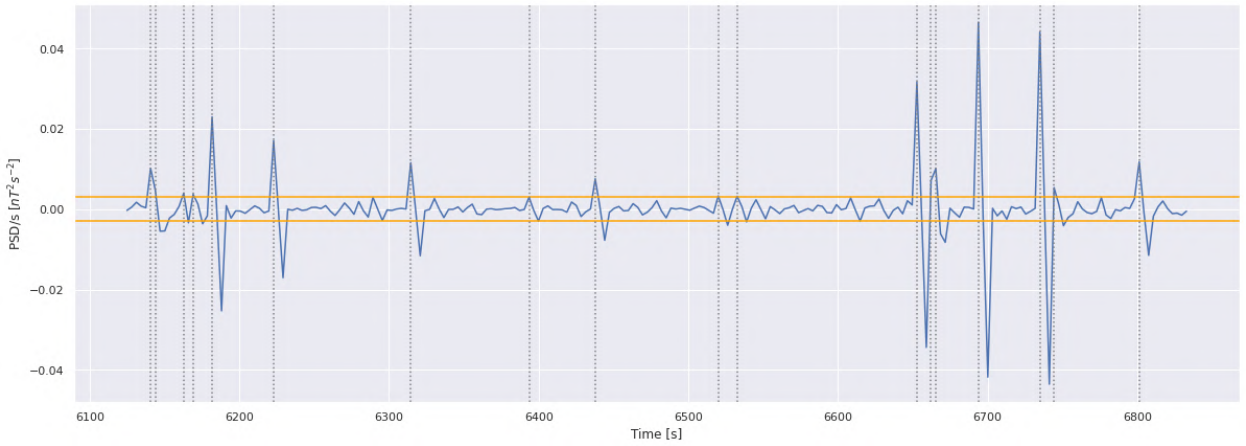


Figure 14: Example of a Region I section for identification of boundaries. The plot corresponds to applying a discrete differentiation to the integrated spectrum of the highlighted band in the Fourier spectrogram in figure 7. The threshold value is represented in orange, and the splittings proposed are shown based on the variations in the derivative that exceed the threshold value in magnitude. The threshold used is $\eta = 0.03$.

# B Directional analysis

For the data gathered crossing the bow shock from the solar wind to the magnetosheath in Region II a splitting in time is made to find the points where discontinuities affect the Fourier windowed spectrogram. Each section is plotted in a $\phi vs \theta$ plane as a contour plot using Kernel Density Estimation.

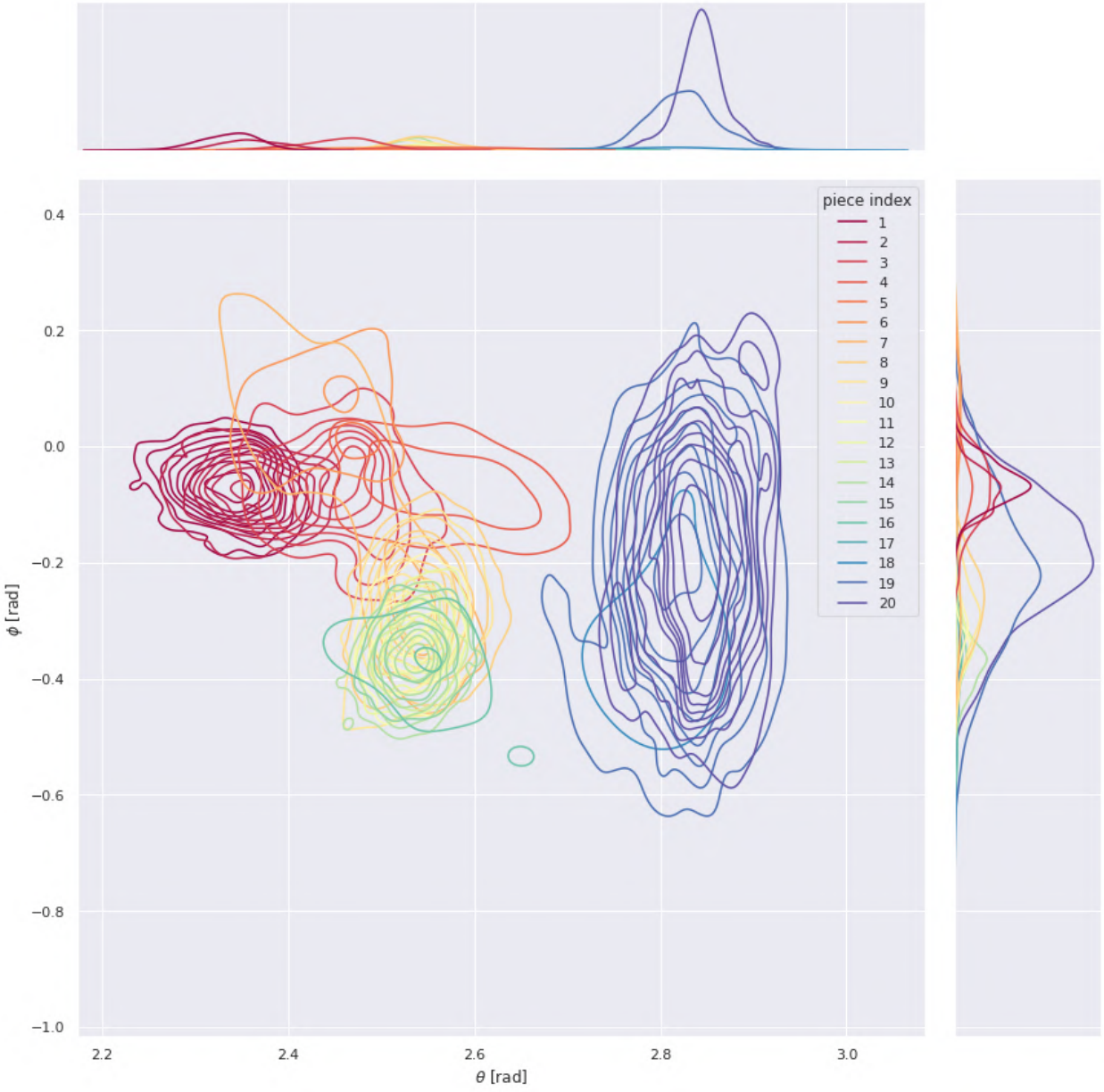


Figure 15: Kernel density estimation contours for the points in the direction plane $\phi$ vs $\theta$ of each section resulting form the splitting made in 10. The Section used corresponding to the Boundary is section 16. Take into account that sections 16-20 correspond to the magnetosheath while sections 0-16 correspond to the solar wind region.